J. Fluid Mech. (2003), *vol.* 478, *pp.* 325–343.
DOI: 10.1017/S0022112002003476 Printed in the United Kingdom

Three-dimensional wave effects on a steady current

By J. GROENEWEG[1] AND J. A. BATTJES[2]

[1]WL|Delft Hydraulics, PO Box 177, 2600 MH Delft, The Netherlands

[2]Delft University of Technology, Faculty of Civil Engineering and Geosciences, PO Box 5048, 2600 GA Delft, The Netherlands

(Received 18 July 2000 and in revised form 23 October 2002)

Measurements in a laboratory flume have shown unexpected wave-induced changes in the vertical profile of the mean horizontal velocity. Two theoretical explanations for these changes have been proposed so far. One is based on a local force balance in the longitudinal direction and the other relies on secondary circulations in the cross-sectional plane. In this study, a two-dimensional (2DV lateral) model based on the so-called generalized Lagrangian mean (GLM) formulation has been developed to investigate the three-dimensional effect of waves on the steady current and in particular to investigate the validity of the two fundamentally different explanations. Formulations for the three-dimensional wave-induced driving force have been implemented in an existing 2DV non-hydrostatic numerical flow model. Computations for regular waves following and opposing a turbulent current over a horizontal bed have been carried out and the results are compared with both experimental results and results from an existing numerical model. The results clearly indicate predominance of the longitudinal component of the wave-induced driving force over the cross-sectional components. Although the 2DV model has only been applied to and verified with measurements in wave–current systems in a laboratory flume, the approach followed here is relevant for a wider class of problems of wave–current interactions.

1. Introduction

Understanding the mechanisms of wave–current interaction is of importance for prediction of vertical profiles of horizontal velocities. This is relevant both from a hydrodynamic point of view (bed friction) and a morphodynamic point of view. Laboratory flume experiments (e.g. Kemp & Simons 1982, 1983; Klopman 1994) showed unexpected wave-induced changes in the profile of the mean horizontal velocity. For waves following the current, the mean horizontal velocity is reduced near the free surface and reaches a maximum at some lower elevation. In the situation of opposing waves, the mean horizontal velocity grows more rapidly towards the free surface than the logarithmic profile (see figure 1).

To our knowledge only two theoretical models have been presented to explain these effects. Nielsen & You (1996) presented a one-dimensional (1DV) model relying on a local force balance in the streamwise direction, in which lateral variations have been neglected. Assuming linear wave theory, expressions were derived for the mean wave contributions to the stresses. These depend on the wave decay. Although their model gives a qualitative explanation, quantitative agreement with Klopman's results was

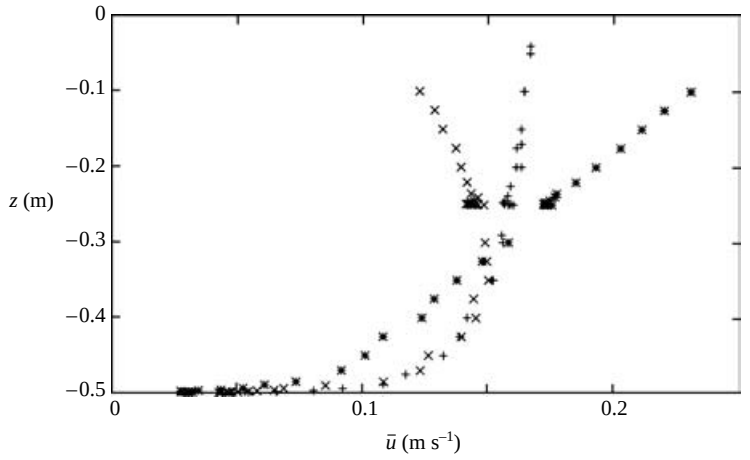

FIGURE 1. Eulerian-mean velocity profiles for the situation of no waves (+) following waves (×) and opposing waves (*) of the same size (depth 0.5 m, wave period 1.44 s, wave amplitude 0.06 m). After Klopman (1994).

obtained only after a significant *ad hoc* enhancement of the wave-induced shear stress $\langle \tilde{u}\tilde{w} \rangle$ by a depth-dependent empirical factor.

Groeneweg & Klopman (1998, hereinafter referred to as GK98) developed a 1DV model based on the generalized Lagrangian mean (GLM) approach. For waves following and opposing a turbulent current, the 1DV model of GK98 provided mean horizontal velocity profiles which agreed quantitatively with the measured profiles of Klopman (1994).

A fundamentally different explanation has been given by Dingemans *et al.* (1996), who presented a two-dimensional (2DV lateral) model in which secondary circulations in the cross-sectional plane were held responsible for the mean velocity profile changes. These circulations, consisting of counter-rotating vortices with their axes in the streamwise direction, are ascribed to the so-called Craik–Leibovich (CL) vortex force. To investigate the existence of secondary circulations, Klopman (1997) repeated the experiments of Klopman (1994). He measured secondary circulations of which the lateral and vertical velocity components are of the same order as the wave-induced second-order changes of the longitudinal velocity.

An intriguing point is that the two models of Nielsen & You (1996) and GK98 assume that changes of the mean horizontal velocity profile are purely caused by phenomena in the longitudinal direction, whereas Dingemans *et al.* (1996) suppose the secondary lateral circulations to be the cause of changes in the mean horizontal velocity profile in the streamwise direction. The purpose of this study is to investigate the relative importance of these two contributions. To this end, a 2DV model has been formulated. Like GK98, this model is based on the so-called GLM formulation. Although the specific elaboration has been carried out for a wave–current system in a laboratory flume (with sidewall influence), the question raised here and the approach that is followed are relevant to a wider class of problems of wave–current interactions.

In § 2 the existence of secondary circulations and their possible effects on the mean horizontal velocity are highlighted. The formulation of the numerical 2DV lateral model, based on the GLM theory, is given in § 3. The 2DV-GLM equations have been implemented in the numerical solver, also used by Dingemans *et al.* (1996),

which is described briefly in § 4. The model verification is presented in § 5, where the model results are compared with laboratory flume measurements. Furthermore, the influence of the width/depth ratio has been investigated in that section. In § 6, a qualitative explanation of the wave-induced vertical profile changes of the mean longitudinal velocity is given.

2. Secondary circulations

Because of the finite channel width, secondary circulations will arise in a current and/or wave flume. For steady flow without waves these are ascribed to asymmetries in the turbulent stresses. Nezu & Nakagawa (1993 chapter 5) observed secondary circulation cells for various aspect ratios, i.e. width to depth ratios.

These circulation cells have also been observed in laboratory flume experiments for the combined motion of waves and current, see e.g. Nepf & Monismith (1991) and, more recently, Nepf *et al.* (1995), Klopman (1997) and Melville, Shear & Veron (1998). Besides the velocity components in the cross-sectional plane, Nepf *et al.* (1995) and Klopman (1997) measured the longitudinal velocity component as well.

A possible explanation for the occurrence of the secondary circulations is based on the CL theory. The CL mechanism was originally suggested by Craik (1977) and is based on a mechanism of instability and feedback. Leibovich (1977) showed that the mean horizontal Eulerian velocity $\overline{u}$ and the Stokes drift $\overline{u}^S$ must decay in the vertical direction z in order for the stability-feedback mechanism to occur. He remarked that the system is stable if

$$\frac{\partial \overline{u}}{\partial z}\frac{\partial \overline{u}^S}{\partial z} < 0 \tag{2.1}$$

over the entire depth, and is unstable otherwise. For an extensive description of the CL2 mechanism, see the original description of Leibovich (1977) or his review paper (Leibovich 1983).

Note that stability criterion (2.1) is valid for laterally uniform Stokes drift velocity and longitudinal mean current. In a finite-width channel these velocities are not uniform. Nepf & Monismith (1991) remarked that in a finite-width channel sidewall boundary layers provide a permanent source of vertical vorticity. Consequently, vertical shear in the current is not critical to the generation of secondary circulations in the flume. In other words, in a finite-width flume, secondary circulations may be produced, despite the fact that stability criterion (2.1) is fulfilled. This is in line with observations by Nepf & Monismith (1991), Nepf *et al.* (1995 p. 16 211) and Klopman (1997).

The wave-induced CL driving force is given by $\boldsymbol{T} = \overline{\boldsymbol{u}}^S \times \overline{\Omega}$ with $\overline{\Omega} = \nabla \times \overline{\boldsymbol{u}}$ the mean vorticity. Craik (1982) gave an approximation of $\boldsymbol{T}$ which is valid for a flume,

$$\boldsymbol{T} \approx \boldsymbol{T}_0 = \left(0, \overline{u}^S \frac{\partial \overline{u}}{\partial y}, \overline{u}^S \frac{\partial \overline{u}}{\partial z}\right)^{\mathrm{T}}. \tag{2.2}$$

with y the spanwise coordinate. In a laboratory flume, the longitudinal velocity increases in the lateral direction from the sidewall to the centre of the flume. The driving force (2.2) indicates that the flow is accelerated laterally towards the plane of maximal longitudinal velocity, if the waves are propagating in the same direction as the current ('following waves'). The acceleration is thus towards the centre of the flume and is strongest near the surface, so that downwelling occurs by continuity. If

the source of longitudinal vorticity is as predicted in the CL equations, vortices with the opposite sense of rotation will be produced if waves are opposing the current.

Dingemans *et al.* (1996) considered the CL driving force (2.2) as a sole driving mechanism for the mean motion. This mechanism for the changes of the mean longitudinal velocity profile is dependent on the existence of secondary circulation cells. This differs from the 1DV explanation of Nielsen & You (1996) and GK98 in which lateral uniformity has been assumed. In the 1DV model of GK98, the driving force for the mean motion is dominated by its longitudinal component. In the following, a 2DV lateral model will be developed in which all three components of the wave-induced driving force are included. In this way, the effect of the secondary circulations on the mean longitudinal velocity can be compared with the direct influence of the longitudinal component of the driving force.

3. Formulation of a 2DV model in the GLM setting

3.1. *Generalized Lagrangian mean formulation*

For the definition of the GLM theory we refer to Andrews & McIntyre (1978), and for an introductory outline to McIntyre (1980) and Dingemans (1997 note 2.10.6). Here, only the essential idea of the GLM theory is outlined. The GLM formulation is used to describe the interaction of waves and currents. In contrast to the more conventional Eulerian formulation, the GLM description enables splitting of the mean and oscillating motion over the whole depth in an unambiguous and unique way, also above wave trough level. The GLM equations are a mapping of the Navier–Stokes equations into a material frame. They provide a very general Lagrangian-mean description of the back effect of oscillatory disturbances upon the mean state and depict a Lagrangian-mean velocity field about which fluctuating particle motions have zero mean, when a temporal, spatial, ensemble or other averaging process is applied. Moreover, provided the mapping is invertible, the equations are exact and thus valid for waves of all amplitudes, although for practical purposes they have so far been restricted to waves of small amplitude.

A Cartesian coordinate system (x, y, z) is used, where z is the vertical coordinate, and x and y are the horizontal coordinates in longitudinal and lateral direction, respectively. The mapping $\boldsymbol{x} \rightarrow \boldsymbol{x} + \boldsymbol{\xi}(\boldsymbol{x}, t)$ is central in the GLM description. Here, $\boldsymbol{\xi}(\boldsymbol{x}, t)$ is a field denoting the disturbance displacement about the position $\boldsymbol{x}$. By introducing $\varphi^{\xi}(\boldsymbol{x}, t) = \varphi(\boldsymbol{x} + \boldsymbol{\xi}(\boldsymbol{x}, t), t)$ for an arbitrary particle-related function φ, Andrews & McIntyre (1978) define a Lagrangian mean operator $\overline{(\,)}^{L}$ by

$$\overline{\varphi(\boldsymbol{x}, t)}^{L} = \overline{\varphi^{\xi}(\boldsymbol{x}, t)}, \tag{3.1}$$

where in our case $\overline{(\,)} = \langle(\,)\rangle$ is a time-average operator. This implies that the average assigned to the fixed point $\boldsymbol{x}$ is taken over disturbed positions $\boldsymbol{x} + \boldsymbol{\xi}(\boldsymbol{x}, t)$. In order that $\boldsymbol{\xi}$ is a true disturbance, it is required that $\overline{\boldsymbol{\xi}(\boldsymbol{x}, t)} = 0$. The disturbance velocity $\boldsymbol{u}^{\ell}$ is defined in a natural way as $\boldsymbol{u}^{\ell} = \boldsymbol{u}^{\xi} - \overline{\boldsymbol{u}}^{L}$, and thus $\overline{\boldsymbol{u}^{\ell}} = 0$. Furthermore, in terms of the Lagrangian-mean material derivative $\overline{\mathrm{D}}^{L} = \partial/\partial t + \overline{u}_j^{L}\partial/\partial x_j$ (the use of repeated indices in one factor implies summation), it follows that

$$\overline{\mathrm{D}}^{L}\boldsymbol{\xi} = \boldsymbol{u}^{\ell}. \tag{3.2}$$

Finally, the difference between the GLM velocity and Eulerian mean velocity is given by the so-called Stokes drift, $\overline{\boldsymbol{u}}^{S} = \overline{\boldsymbol{u}}^{L} - \overline{\boldsymbol{u}}$. A Stokes correction $\overline{\varphi}^{S}$ can be expressed in terms of fluctuating quantities. In e.g. GK98 (p. 291), a second-order approximation

has been given,

$$\overline{\varphi}^S(\boldsymbol{x},t) \equiv \overline{\varphi}^L(\boldsymbol{x},t) - \overline{\varphi}(\boldsymbol{x},t)$$
$$= \left\langle \xi_j \frac{\partial}{\partial x_j}\left(\varphi^\ell - \xi_k \frac{\partial \overline{\varphi}^L}{\partial x_k}\right)\right\rangle + \tfrac{1}{2}\langle \xi_j \xi_k\rangle \frac{\partial^2 \overline{\varphi}^L}{\partial x_j \partial x_k} + O(a^3). \tag{3.3}$$

3.2. *Derivation of the 2DV-GLM equations in a cross-sectional plane*

The 2DV model presented here is based on the three-dimensional GLM equations derived by GK98. The lateral 2DV model provides a local solution in a cross-sectional plane and is derived in the following by neglecting variations in the longitudinal direction of GLM quantities in the general three-dimensional GLM equations, except for the hydrostatic part of the longitudinal pressure gradient, which is related to the GLM surface elevation $\overline{\zeta}^L$. The total pressure $\overline{p}^L$ is decomposed into a hydrostatic and non-hydrostatic part, $\overline{p}^L = \rho g(\overline{\zeta}^L - z) + \overline{\pi}^L$.

Using the summation convention, Latin (in italic) indices denote all three coordinates x, y, z. Greek indices denote only the lateral and vertical coordinates y and z. Assuming a constant density ρ, the continuity equation and the three momentum equations read

$$\frac{\partial \overline{u}_\alpha^L}{\partial x_\alpha} = -\overline{\mathrm{D}}^L(\log J), \tag{3.4}$$

$$\frac{\partial \overline{u}_i^L}{\partial t} + \overline{u}_\alpha^L \frac{\partial \overline{u}_i^L}{\partial x_\alpha} + \frac{1}{\rho}\frac{\partial \overline{p}^L}{\partial x_i} - \frac{1}{\rho}\frac{\partial \overline{\tau}_{i\alpha}^L}{\partial x_\alpha} = \overline{S}_i^L. \tag{3.5}$$

Here, J is the Jacobian of the mapping $\boldsymbol{x} \to \boldsymbol{x} + \boldsymbol{\xi}$, i.e. $J = \det(\partial \Xi_j/\partial x_i)$, with $\boldsymbol{\Xi} = \boldsymbol{x} + \boldsymbol{\xi}$ the disturbed position, and τ_{ij} denotes the stress tensor components, which are directly related to the strain rates using the Boussinesq hypothesis. A turbulence model is required to determine the eddy viscosity ν and provide proper closure of the flow equations. The pressure gradient is given by $\nabla \overline{p}^L = (\rho g \partial \overline{\zeta}^L/\partial x, \rho g \partial \overline{\zeta}^L/\partial y + \partial \overline{\pi}^L/\partial y, \partial \overline{\pi}^L/\partial z - \rho g)$. The longitudinal gradient of the hydrostatic pressure, $\partial \overline{\zeta}^L/\partial x$, is assumed constant over each cross-section and is chosen such that the discharge of the combined flow equals the discharge Q of the flow without waves,

$$Q = \int_{-L}^{L}\int_{-h}^{\overline{\zeta}^L} \overline{u}^L \,\mathrm{d}z\,\mathrm{d}y. \tag{3.6}$$

Here, the width of the channel is equal to $2L$. The GLM free-surface elevation $\overline{\zeta}^L$ is determined from the continuity equation. Integration of (3.4) over depth and substitution of the boundary conditions for the vertical GLM velocity,

$$\overline{w}^L = \overline{\mathrm{D}}^L \overline{\zeta}^L \quad \text{at } z = \overline{\zeta}^L, \tag{3.7a}$$

$$\overline{w}^L = -\overline{\mathrm{D}}^L h \equiv 0 \quad \text{at } z = -h, \tag{3.7b}$$

yields

$$\frac{\partial \overline{\zeta}^L}{\partial t} + \frac{\partial}{\partial x}\left(\int_{-h}^{\overline{\zeta}^L} \overline{u}^L \,\mathrm{d}z\right) + \frac{\partial}{\partial y}\left(\int_{-h}^{\overline{\zeta}^L} \overline{v}^L \,\mathrm{d}z\right) = -\int_{-h}^{\overline{\zeta}^L} \overline{\mathrm{D}}^L(\log J)\,\mathrm{d}z. \tag{3.8}$$

Since longitudinal variations of GLM quantities are neglected, the second term in the left-hand side of (3.8) vanishes.

On the right-hand side of (3.5), $\overline{\boldsymbol{S}}^L$ denotes the wave-induced driving force, given by

$$\overline{S}_i^L = \frac{1}{\rho}\frac{\partial \overline{p}^S}{\partial x_i} - \frac{1}{\rho}\frac{\partial \overline{\tau}_{ij}^S}{\partial x_j} - \frac{\partial r_{ij}}{\partial x_j}. \tag{3.9}$$

The tensor r_{ij} contains the wave-induced stress in terms of Lagrangian quantities and is given by

$$r_{ij} = \overline{u_i^\ell u_j^\ell} - \overline{\mathrm{D}}^L\left(\overline{u_i^\ell \xi_j}\right). \tag{3.10}$$

In (3.9), the Stokes corrections of the pressure $\overline{p}^S$ and $\overline{\tau}_{ij}^S$ can be expressed in disturbance-related variables. Once these wave quantities are known, the wave-induced driving force can be determined and the mean flow equations, (3.5), can be solved.

Several sources of non-zero wave-induced shear stresses $\langle u'w' \rangle$ for flow over a horizontal bed have been described in the literature, such as the vorticity generation and diffusion in the bottom boundary layer (Longuet-Higgins 1953), nonlinear vorticity transfer from the current to the wave motion (Peregrine 1976) and wave decay (see e.g. Deigaard & Fredsøe 1989). The Stokes correction of the shear stress $\overline{\tau}_{xz}^S$ can be interpreted as a wave-induced imbalance term of the shear stress. It is significant in regions where the fluctuating part of the shear stress τ_{xz}^ℓ is changing rapidly over depth. Obviously, this is in the regions near the bed and the free surface.

The disturbance-related quantities, like $\boldsymbol{\xi}$ and $\boldsymbol{u}^\ell$, scale with the wave motion, which has amplitude a. This wave amplitude is supposed to be small with respect to both depth and wavelength. Despite the fact that a is not dimensionless, the order of approximation is denoted by $O(a^n)$. GK98 derived the following equation for the fluctuating motion:

$$\overline{\mathrm{D}}^L u_i^\ell + \frac{1}{\rho}\frac{\partial}{\partial x_i}\left(p^\ell - \xi_j \frac{\partial \overline{p}^L}{\partial x_j}\right) - \frac{1}{\rho}\frac{\partial}{\partial x_j}\left(\tau_{ij}^\ell - \xi_k \frac{\partial \overline{\tau}_{ij}^L}{\partial x_k}\right) = \xi_j \frac{\partial}{\partial x_j}\left(\overline{\mathrm{D}}^L \overline{u}_i^L\right) + O(a^2). \tag{3.11}$$

The flow equations (3.5) and (3.11) are coupled. Consequently, they should be integrated simultaneously. For the development of their 1DV model, GK98 applied a WKBJ perturbation series analysis to the three-dimensional GLM-based flow equations. A perturbation series approach has not been used in the present 2DV model. In fact, the total mean motion is considered. Therefore, $\overline{\boldsymbol{S}}^L$ must be evaluated at each time step of the numerical integration procedure. For that purpose, expressions for the fluctuating quantities are required. These will be determined with the 1DV model of GK98. According to the WKBJ perturbation series approach, the fluctuating quantities depend on the initial current instead of the instantaneous current. Hence, the part of the driving force that is expressed completely in terms of fluctuating quantities is influenced by the initial current instead of the total mean motion. This inconsistency in the model is not expected to have significant consequences. The direct influence of the mean motion within the wave-induced driving force is larger than the indirect effect of the mean motion through the fluctuating quantities.

3.3. *Sidewall effects on fluctuating quantities*

In the GK98 1DV model, laterally uniform vertical distributions of oscillatory quantities have been determined. In order to take sidewall effects into account, a procedure has been adopted here that was also used by Mei, Liu & Carter (1972, appendix I). By neglecting the influence of the mean current and variations of the eddy viscosity ν in the sidewall boundary layers, they showed that the orbital velocity

including the no-slip condition at the sidewalls satisfies Stokes' shear wave solution,

$$\boldsymbol{u}^{\ell} = [1 - \exp(\beta Y)]\boldsymbol{u}_1^{\ell}, \tag{3.12}$$

with $\beta = (-\mathrm{i}\omega_0/\nu)^{1/2}$, Y the distance to the nearest sidewall and $\boldsymbol{u}_1^{\ell}$ the 1DV solution which holds outside the sidewall boundary layer. The complex-valued β is responsible for phase and amplitude changes in the sidewall layer. This model is also applied here.

The distribution of the wave-induced driving forces in the entire cross-section can now be evaluated easily by substituting the laterally and vertically varying oscillating quantities in the general expressions for the driving forces. Note that the vertical variations are obtained from the 1DV model, see GK98.

4. Numerical solution method

In Van Kester, Uittenbogaard & Dingemans (1996) several solution techniques were investigated to solve the 2DV flow equations. They concluded that the pressure correction method of Casulli (1995) was the best for problems dealing with the combined motion of waves and currents. This method has also been selected for the present purpose. It is described in § 4.1. The implementation of the 2DV-GLM equations in a numerical flow model is given in § 4.2.

4.1. *Pressure correction method*

Casulli & Stelling (1998) applied the pressure correction method for the numerical integration of the full Reynolds-averaged Navier–Stokes equations for simulating large-scale non-hydrostatic flows. This is a fractional step method, in which the hydrostatic and the hydrodynamic component of the pressure are considered separately. Reference is made to Casulli & Stelling (1998) for the numerical implementation and properties of the fractional step method introduced by Casulli (1995). The solution procedure consists of two stages.

Stage 1

The depth-integrated continuity equation (3.8) and the momentum equations (3.5) are considered with $\overline{\pi}^L \equiv 0$. This differs from the usual approach in a shallow-water model where the vertical velocity is obtained from the continuity equation. Consequently, the velocity field does not necessarily satisfy the continuity equation (3.4) after the first stage. The resulting shallow-water equations are integrated following the integration schemes of Delft Hydraulics' models Delft3D-Flow, (WL|Delft Hydraulics 1999), for a complete time step. For stability reasons, the vertical advection and a part of the vertical shear stress terms are treated implicitly.

Stage 2

The momentum equations are considered without the convective terms and only the hydrodynamic pressure is taken into account,

$$\frac{\partial \overline{u}_i^L}{\partial t} + \frac{1}{\rho}\frac{\partial \overline{\pi}^L}{\partial x_i} = 0. \tag{4.1}$$

By taking the divergence of (4.1) and applying the continuity equation as a side condition, a Poisson equation for the hydrodynamic pressure is obtained. The conditions of zero normal flow at the bottom and sidewalls and a vanishing hydrodynamic pressure at the free surface provide a unique solution. A second-order discretization on a rectangular grid leads to a system of equations, with a

symmetric positive-definite matrix, that is solved with the preconditioned conjugate gradient method. The second stage is completed after substitution of $\overline{\pi}^L$ in (4.1), resulting in a new estimate for the velocity components.

4.2. *Implementation of 2DV-GLM equations in a numerical flow model*

The pressure correction method described above has been implemented in a numerical code by Van Kester *et al.* (1996), see also Dingemans *et al.* (1996). Whereas in the 1DV model, as used by GK98, the bottom boundary layer is resolved, using a no-slip condition at the bed, Dingemans *et al.* (1996) imposed partial-slip conditions at the bottom and the sidewall boundaries, using a logarithmic law-of-the-wall formulation. Given a shear velocity at a certain distance from the wall, the friction velocity and related shear stress are determined, following Grant & Madsen's (1979) formulation. This formulation is given in a Eulerian framework. In order to obtain the GLM shear stress at a closed boundary, the following algorithm has been applied:

(i) The GLM velocity at a small distance from the boundary is transformed to its Eulerian equivalent at the same distance by subtracting the Stokes drift velocity.

(ii) The formulation of Grant & Madsen (1979) as implemented by Dingemans *et al.* (1996) is used to determine the Eulerian shear stress.

(iii) The GLM shear stresses are obtained by adding the Stokes correction of the shear stresses to the Eulerian shear stresses.

Finally, for simulating turbulent flow, a turbulence model must be implemented. Any of the turbulence models implemented by Van Kester *et al.* (1996) can be used. In a first approach, a classical turbulence model has been used. For this study we chose a $k-\varepsilon$ model, in which the eddy viscosity is the same for all turbulent Reynolds stresses (isotropic eddy viscosity). For closure of the turbulence model, the production term is computed with Eulerian velocities, which are determined by transforming the GLM velocities. A description of the turbulence model is given in the Appendix.

5. 2DV model computations

5.1. *Verification of the 2DV model*

For situations of following and opposing waves, the mean velocities have been computed and compared with the laboratory flume measurements of Klopman (1997). The conditions in these experiments are identical to those of Klopman's (1994) measurements concerning regular waves in a turbulent current. The channel is 45 m long and 1 m wide. The bed was roughened using coarse sand with a grain size of about 2 mm. Laser Doppler velocimetry (LDV) flow metres have been used to measure longitudinal and vertical velocities at a measuring section 22.5 m away from the wavemaker. Since the bed is neither smooth nor rough, the flow is in the intermediate turbulent regime.

A flow-circulation circuit provided a turbulent current with a constant discharge $Q = 0.08\,\mathrm{m^3\,s^{-1}}$ in a flume with a still-water depth $h = 0.50\,\mathrm{m}$ (cross-sectionally averaged flow velocity $0.16\,\mathrm{m\,s^{-1}}$). A monochromatic wave field with a wave period $T = 1.44\,\mathrm{s}$ and an initial wave amplitude $a = 0.060\,\mathrm{m}$ is imposed on the current. From the measurements, the bed roughness parameter z_0 was estimated at 0.037 mm. Klopman (1997) measured vertical and longitudinal velocities in 30 points in half a cross-sectional plane, after an initial transient of at least half an hour to make sure that the conditions had sufficiently developed to a steady state. Since the measuring section is 45 water depths away from the wavemaker and current inlet, the measured

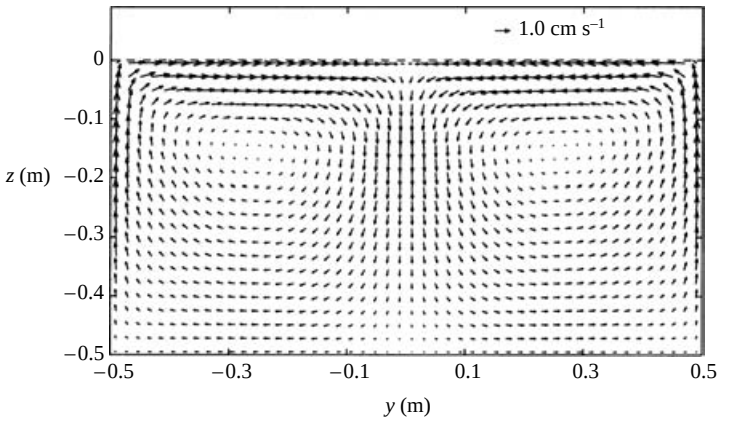

FIGURE 2. Computed mean velocity distribution in a cross-section for waves following the current.

velocities are uniform in longitudinal direction as well. The latter is necessary for comparison with the 2DV lateral model. Klopman determined the lateral mean velocity afterwards by continuity.

In the present 2DV model, the wave-induced driving forces include a factor $\beta = (-i\omega/\nu)^{1/2}$. In our analysis, ν was assumed to be independent of the distance to the wall. We have taken $\nu = 10^{-5}\,\mathrm{m^2\,s^{-1}}$ for all experiments, based on the order of magnitude of ν in the turbulent bottom boundary layer. This value for ν leads to a thickness of the sidewall boundary layer of the order 0.5 cm.

For the spatial discretization, a computational grid of 100 points in the lateral direction and 40 points in the vertical has been used. In both directions, the grid refinement procedure of Vinokur (1983) was applied, such that 3 to 4 grid points are inside the boundary layers, including the one near the bottom. The time step for the simulations is 0.01 s.

In all 2DV model computations, a current-only situation has been considered in the first 200 s. After 200 s ($t = 0$), the wave influence on the mean motion is taken into account by activating the wave-induced driving force. Since velocity measurements have been carried out at fixed locations and are thus Eulerian, the GLM velocity field $\overline{\boldsymbol{u}}^L$ has to be transformed to its corresponding Eulerian field, $\overline{\boldsymbol{u}} = \overline{\boldsymbol{u}}^L - \overline{\boldsymbol{u}}^S$, for comparison. The lateral and vertical components of the Stokes drift $\overline{\boldsymbol{u}}^S$ have been neglected.

The situation of waves following the turbulent current is considered first. The computed mean velocity vectors in a cross-section are shown in figure 2. For clarity in the plot, the lateral and vertical velocity components have been interpolated (bi-linear interpolation) to points which form a regular grid. Both the computed and measured vertical profiles of the mean vertical velocity at $y = 45$ cm, $y = 30$ cm and $y = 1.5$ cm (near the centre of the flume) are shown in figure 3. These computed profiles represent the steady solution obtained at $t = 600$ s.

Figure 2 shows that the 2DV model predicts two counter-rotating vortices, both occupying half of the cross-section. The two vortex axes are approximately 15 cm below the mean free surface, or approximately 10 cm above mid-depth. The cross-sectional velocity computed with the present 2DV model agrees qualitatively with the measured velocity components, but quantitatively the agreement is far from perfect

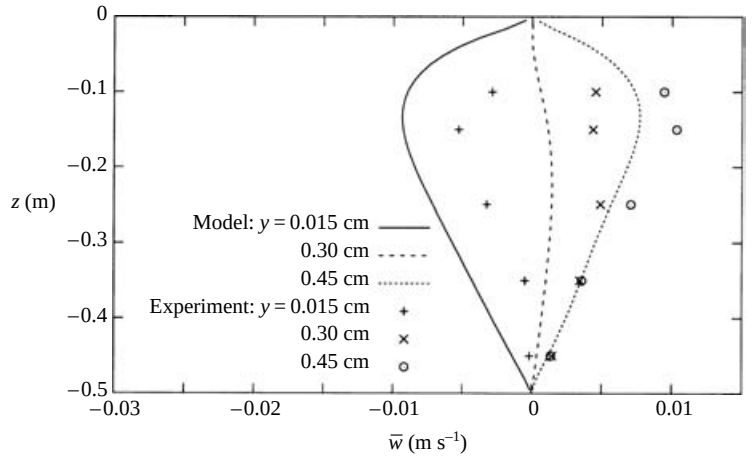

FIGURE 3. Computed and measured (Klopman 1997) mean vertical velocity profiles at different distances y from the flume centre (following waves).

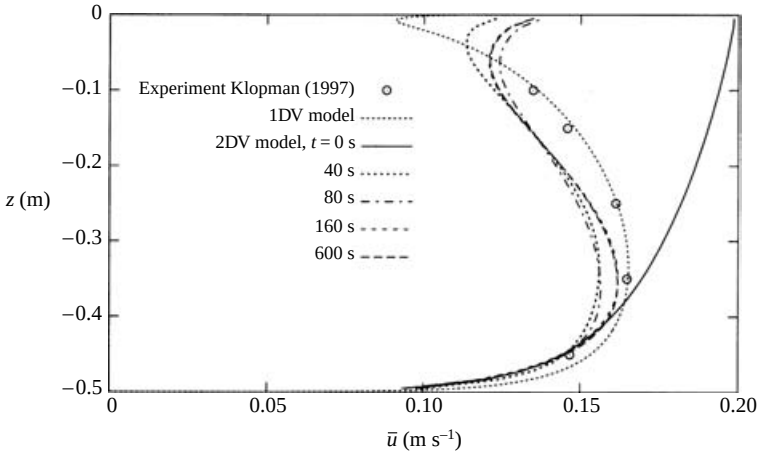

FIGURE 4. Computed (1DV and 2DV model) and measured vertical profiles of the mean longitudinal velocity in the centre of the flume at various times (following waves).

(figure 3). The downwelling in the centre of the flume ($y = 1.5$ cm) is overpredicted by a factor 2.

The influence of the wave motion on the mean motion is significant. Mean longitudinal velocity profiles in the flume centre are given in figure 4 for various times. Comparison of the velocity profiles for $t = 0$ (current alone) and $t > 0$ shows a significant reduction of the mean longitudinal velocity towards the free surface, even stronger than was measured by Klopman (1997) and by the model of Dingemans *et al.* (1996 figure 4). In figure 4, the 2DV model results are compared with the prediction of the 1DV model of GK98 as well. Because of the sidewall resistance, the depth-averaged longitudinal velocity in the centre of the flume is larger than the longitudinal velocity averaged over the entire cross-section, i.e. $0.16\,\mathrm{m\,s^{-1}}$. Therefore, the 1DV model computations have been carried out prescribing a depth-averaged longitudinal GLM velocity of $0.166\,\mathrm{m\,s^{-1}}$, being the depth-averaged longitudinal

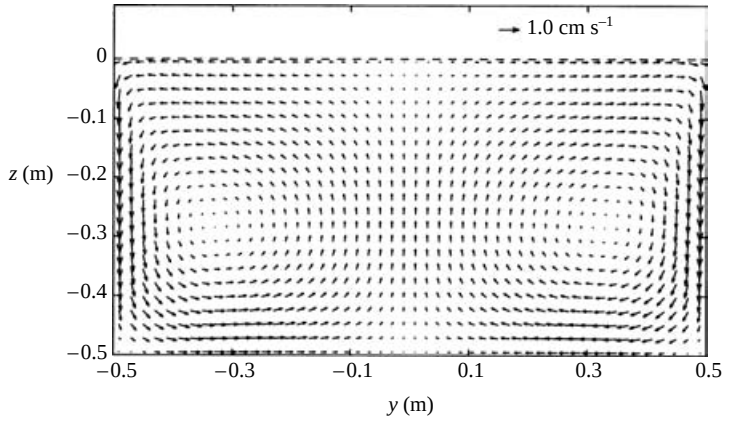

FIGURE 5. Computed mean velocity distribution in cross-section for waves opposing the current.

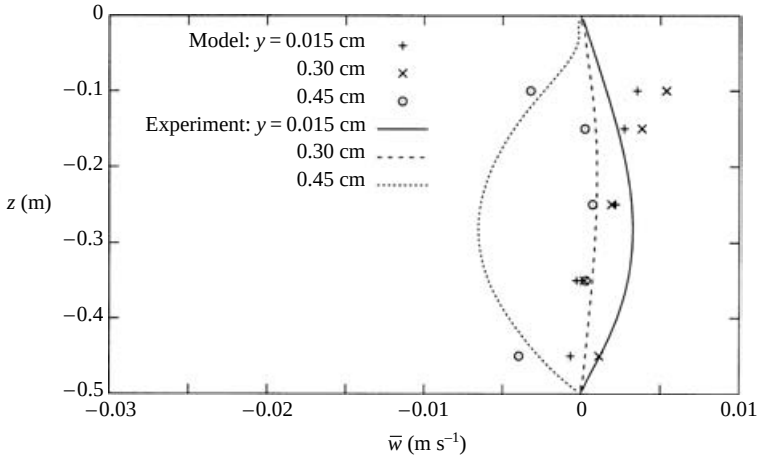

FIGURE 6. Computed and measured (Klopman 1997) mean vertical velocity profiles at different distances y from the flume centre (opposing waves).

GLM velocity in the centre flume computed by the 2DV model. The 1DV model results appear to be in better agreement with the measurements than the 2DV results. The reasons for this are not clear.

For waves propagating against the current, the computed steady secondary flow is presented in figure 5. The vortices now rotate in the opposite direction to those for the case of following waves. The cell centres are displaced slightly downward and towards the sidewalls. Figure 6 shows that despite the fact that the maximum of the vertical velocity is predicted correctly, quantitative agreement between the measured and computed profiles of the vertical velocity has not been obtained.

Although the intensity of the secondary circulations is not predicted correctly, the computed profile of the mean longitudinal velocity is in good agreement with the measured profile, as can be seen in figure 7. Compared to the situation without waves, the mean longitudinal velocity reduces near the bed and increases significantly towards the free surface. The depth-averaged longitudinal GLM velocity in the flume

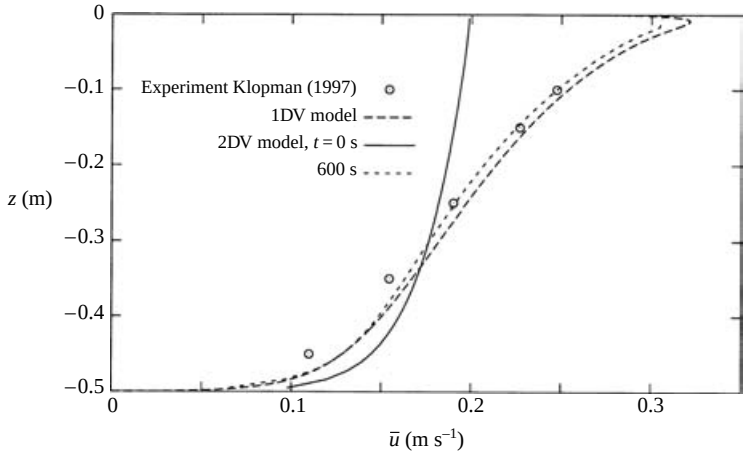

FIGURE 7. Computed (1DV and 2DV model) and measured vertical profiles of the mean longitudinal velocity in the centre of the flume (opposing waves).

centre computed by the 2DV model is $0.181\,\mathrm{m\,s^{-1}}$. The 1DV model computations have been carried out prescribing the same value for the depth-averaged longitudinal GLM velocity. Comparison of the 1DV result with the profile computed by the 2DV model shows good agreement between the two profiles.

An important conclusion is drawn from these tests. The effect of the secondary circulations on the mean longitudinal velocity is noticeable, but weak compared to the effect of longitudinal driving forces.

5.2. *Influence of width/depth ratio*

The effect of the streamwise vorticity will decrease when the flume is widened. The 2DV model solution is then expected to converge to the 1DV solution. To check the consistency of the 2DV model in this regard, identical situations are considered as in the previous subsection, but now in a significantly wider flume. Nepf *et al.* (1995) observed two or more vortex pairs in a laboratory flume with aspect ratio 1:8 and 1:12. However, they considered breaking waves on a turbulent current and concluded that the breaker activity not only made the flow more unstable, but also introduced suitable seed vorticity to initiate the CL2 mechanism. The vortices were ultimately maintained through interaction with the bottom boundary layer. For non-breaking waves, the extra vorticity-generating mechanism at the free surface is not present. Only the permanent vertical vorticity in the sidewall boundary layers produce streamwise vorticity. The generated vortices are expected to grow towards the centre of the flume and disintegrate into more pairs of streamwise vortices, owing to instabilities.

Here, a 5 m wide flume is considered (as before, $h = 0.50\,\mathrm{m}$). The discharge is increased proportionally, $Q = 0.40\,\mathrm{m^3\,s^{-1}}$. The computed steady cross-sectional velocity distribution for the situation of waves following the current is given in figure 8. In view of symmetry, only half of the cross-section has been plotted. Near the sidewalls, the computed vertical velocities in the 5 m wide flume are of the same order of magnitude as those in the 1 m wide flume. However, in the centre of the flume, the downwelling has decreased significantly and is at most $1.6\,\mathrm{mm\,s^{-1}}$. The cell centres are located approximately 70 cm away from the sidewall, at the halfway position of

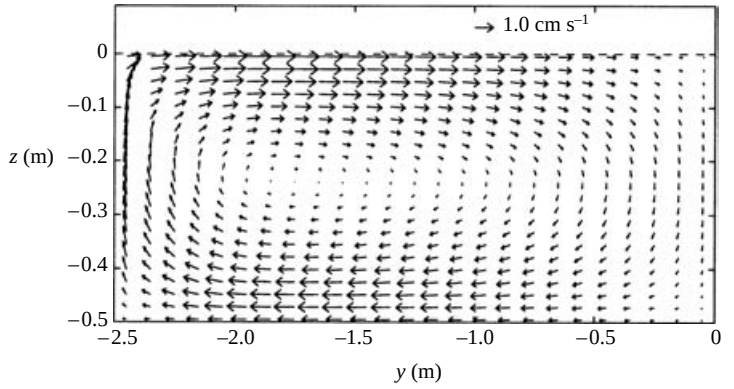

FIGURE 8. Computed mean velocity distribution in the left-hand half of the cross-section for waves following the current in a 5 m wide flume.

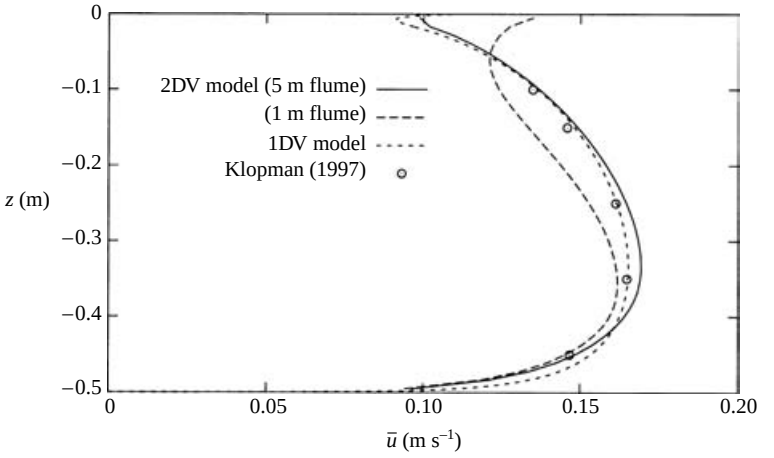

FIGURE 9. Computed mean longitudinal velocity profile in the centre of a 5 m wide flume for waves following the current, compared with measured and computed results in a 1 m wide flume.

the water depth. This is relatively farther away from the flume centre than in the 1 m wide flume.

Our main interest is the mean longitudinal velocity profile in the centre of the flume. The result of the 2DV model computations for the 5 m wide flume is shown in figure 9. In this figure, Klopman's (1997) experimental results as well as the 1DV results and the 2DV model results obtained from the 1 m wide flume (figure 4) have been plotted. Clearly, the vertical profile of the mean longitudinal velocity predicted by the 2DV model converges to its 1DV counterpart.

For the situation of opposing waves, a similar pattern has been observed (not shown here). The secondary circulation consists of two cells for which the centres are located relatively close to the sidewalls. Once again, the vertical velocities near the sidewalls are comparable to those computed for the 1 m wide flume. The maximal upwelling in the centre of the flume is reduced to 0.3 mm s^{-1} and can therefore be neglected.

Comparison of the 1DV result for the longitudinal velocity in the flume centre with the profile computed by the 2DV model for the 5 m wide flume (figure 10) shows

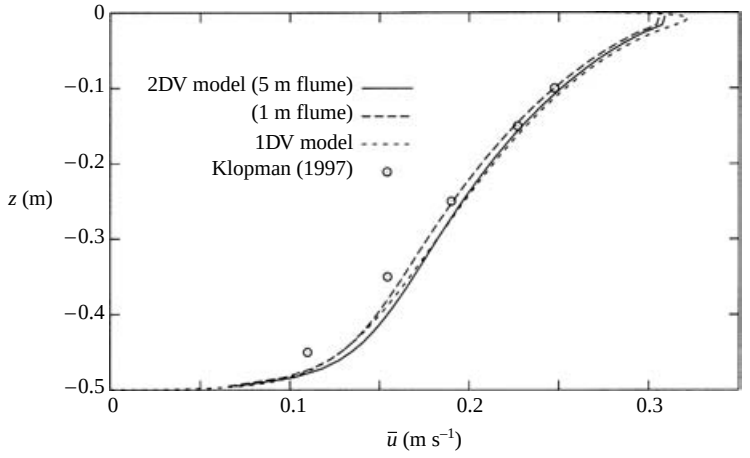

FIGURE 10. Computed mean longitudinal velocity profile in the centre of a 5 m wide flume for waves opposing the current, compared with measured and computed results in a 1 m wide flume.

good agreement. Furthermore, the profiles computed by the 2DV model for the 1 m and 5 m wide flume are almost similar. The computed profile for the 5 m wide flume is slightly closer to the 1DV profile than the 1 m flume profile.

5.3. *Evaluation of model results*

A reasonably good agreement has been obtained between the computed and measured vertical profiles of the mean longitudinal velocities for both situations of waves following and opposing the current. The computed secondary flows (circulation cells) are qualitatively correct, but quantitative agreement with the measured velocities in the cross-sections has not been obtained. This is ascribed to the simplicity of the turbulence model, which does not simulate non-isotropic normal Reynolds stresses and therefore cannot predict circulation cells for a flow without waves.

Despite the fact that the cross-sectional circulations are not computed correctly, the computed and measured longitudinal velocities in the centre of the flume show satisfactory agreement. This implies that the cross-sectional circulations have, at most, a secondary influence on the vertical profile of streamwise velocity.

In contrast to the 2DV GLM-based model, the changes in the predicted longitudinal velocity profiles based on the model of Dingemans *et al.* (1996, figure 4) are entirely due to the secondary circulations. However, both for following and opposing waves, the order of magnitude of the circulation velocity is overpredicted by a factor 3 to 4 in their model, owing to poor estimates of the Stokes drift, and thus the CL vortex force in the boundary layers. Despite these overpredicted circulation velocities, the predicted reduction of the longitudinal surface velocity in the centre of the flume, for the situation of waves following the current, is not as strong as measured. For opposing waves, the predicted mean longitudinal velocity appears to be hardly affected by the waves, except in the lower part where a reduction is predicted. However, this reduction is not as strong as measured.

The preceding observations support the conclusion, stated above, that cross-sectional circulations have, at most, a secondary influence on the vertical profile of streamwise velocity. Furthermore, the longitudinal vortices as such can only be

responsible for the observed changes in the mean longitudinal velocity in the situation of following waves, in which the secondary flow consists of counter-rotating vortices with upwelling along the sidewalls and downwelling in the centre of the flume. Thus, low forward momentum from the sidewalls is transferred along the upper part towards the centre of the flume. Consequently, the mean longitudinal velocity in the upper regions is expected to decrease. However, in the case of opposing waves the vortices rotate in the opposite direction, again transporting low forward momentum to the surface layer, in this case from below. Consequently, the upwelling in the centre of the flume cannot induce the observed increase of the mean longitudinal velocity in the upper part of the flume.

For a realistic prediction of the wave effects on the current velocity profile, the driving force requires a significant component in the longitudinal direction, as is the case in GK98 and in the 2DV model presented herein. This is further supported by the results of the 2DV simulations for the flume that is five times wider. Despite the fact that the secondary circulations in the wider flume are much weaker than in the 1 m wide flume (compare e.g. figures 2 and 8 for following waves), the vertical profile of streamwise velocity in the centre is virtually the same (see figures 9 and 10 for following and opposing waves, respectively). Therefore, it is concluded that the effect of the longitudinal component of the wave-induced driving force on the mean longitudinal velocity is dominant over the influence of the cross-sectional part.

6. Discussion

In GK98, the mean longitudinal velocity profiles observed in laboratory experiments have been simulated reasonably accurately with the 1DV model. The computations in § 5 show that longitudinal vortices seem to have only a minor influence on that velocity component. In this section, a qualitative explanation is given of the observed and calculated changes in the vertical profile of the mean longitudinal velocity, based on the effects of the longitudinal component of the driving forces only, as in the 1DV model.

In a situation without waves, the vertical gradient of the shear stress τ_{xz} (the latter reckoned positive by convention) is in balance with the horizontal gradient of the pressure. Hence, the shear stress varies linearly over depth, vanishing at the free surface. Together with a parabolic eddy viscosity, this leads to a logarithmic distribution in the background current.

Decay of waves in the propagation direction, as in a flume, causes a downward transport of forward momentum in the surface layers, equivalent to a shear stress, with absolute value decreasing with increasing distance beneath the free surface. (This is most obvious for breaking waves.) For waves opposing the current, these wave-induced shear stresses are negative (i.e. they have opposite signs compared to the shear stress due to the ambient current). Therefore, addition of these wave-induced stresses to the undisturbed stress distribution would cause a reduction of the total stresses and a downward decreasing deviation from the linear vertical shear stess variation, which is required to maintain equilibrium with the mean pressure gradient. Therefore, to fulfil this equilibrium condition, the turbulent Reynolds (current-related) shear stresses must increase, the more so as the free surface is approached. As a result, the vertical profile of the mean velocity becomes more strongly sheared towards the free surface. This explains the observed enhancement of the mean velocity near the surface owing to the superposition of waves opposing the current, resulting in an S-shaped profile as observed.

Likewise, waves following the current cause a decrease of the mean velocity gradient and (therefore) of the velocities themselves towards the free surface. This effect is apparently strong enough to even reverse the sign of the gradient, resulting in the observed backward bending of the mean velocity profile in the upper region.

7. Conclusions

A 2DV model has been developed, based on the generalized Lagrangian mean concept, for a coexisting wave–current system in a flume, to investigate the relative importance of longitudinal and cross-sectional contributions to the wave-induced driving force and their influence on the current velocity profile. A key feature of this model is that it contains a significant longitudinal contribution to the wave-induced driving force affecting the mean flow, in contrast to the model based on the CL vortex force presented by Dingemans *et al.* (1996), which relies exclusively on cross-sectional contributions associated with lateral circulations.

The 2DV model presented here appears to predict the wave-induced changes in the vertical profile of streamwise velocity fairly well, both for waves following and opposing the current. The cross-sectional circulations (counter-rotating flows) are correctly predicted in a qualitative sense, but not quantitatively.

The wave-induced changes in the current velocity profile in the centre of the flume, computed with the 2DV model, are insensitive to a five-fold variation in flume width, whereas the cross-sectional circulations are strongly affected.

It is inferred from the preceding conclusions that the longitudinal contribution to the wave-induced driving force is dominant over the cross-sectional contributions. Using the GLM framework, a qualitative explanation is presented for the changes of the vertical profile of the mean longitudinal velocity, for waves decaying in the propagation direction. More specific, vorticity generation and wave decay produce a wave-induced imbalance in the shear stress. This is compensated by changes in the current shear stress, resulting in changes in the vertical distribution of the mean horizontal velocity, as observed.

This work was supported by the Technology Foundation (STW), The Netherlands, and by the Commission of the European Communities, Directorate General for Science, Research and Development (contract no. MAS3-CT97-0081, MAST-project Surf and Swash Zone Mechanics (SASME)). We thank one of the referees for his valuable comments and suggestions.

Appendix. Implementation of k–ε turbulence model

The two-equation k–ε turbulence model provides both the mean turbulent kinetic energy, here denoted as $\overline{q}$, and mean dissipation $\overline{\varepsilon}$ by means of a transport equation with flow dependent source and sink terms. Following Rodi (1980) the transport equations for $\overline{q}$ and $\overline{\varepsilon}$, which are nonlinearly coupled by means of the eddy viscosity ν and the dissipation terms, are given by

$$\frac{\partial \overline{q}}{\partial t} + \overline{v}\frac{\partial \overline{q}}{\partial y} + \overline{w}\frac{\partial \overline{q}}{\partial z} = \frac{\partial}{\partial y}\left(\left(\nu_0 + \frac{\nu}{\sigma_k}\right)\frac{\partial \overline{q}}{\partial y}\right) + \frac{\partial}{\partial z}\left(\left(\nu_0 + \frac{\nu}{\sigma_k}\right)\frac{\partial \overline{q}}{\partial z}\right) + \mathscr{P}_k - \overline{\varepsilon}, \tag{A 1a}$$

$$\frac{\partial \overline{\varepsilon}}{\partial t} + \overline{v}\frac{\partial \overline{\varepsilon}}{\partial y} + \overline{w}\frac{\partial \overline{\varepsilon}}{\partial z} = \frac{\partial}{\partial y}\left(\left(\nu_0 + \frac{\nu}{\sigma_\varepsilon}\right)\frac{\partial \overline{\varepsilon}}{\partial y}\right) + \frac{\partial}{\partial z}\left(\left(\nu_0 + \frac{\nu}{\sigma_\varepsilon}\right)\frac{\partial \overline{\varepsilon}}{\partial z}\right) + c_{1\varepsilon}\frac{\overline{\varepsilon}}{\overline{q}}\mathscr{P}_k - c_{2\varepsilon}\frac{\overline{\varepsilon}^2}{\overline{q}}, \quad \text{(A 1}b\text{)}$$

where ν_0 denotes the kinematic viscosity. The advection and diffusion terms along the flume have been neglected and the eddy viscosity ν and the production term $\mathscr{P}_k$ are given by

$$\nu = c_\mu \frac{\overline{q}^2}{\overline{\varepsilon}}, \quad \text{(A 2)}$$

$$\mathscr{P}_k = 2\nu\left[\left(\frac{\partial \overline{v}}{\partial y}\right)^2 + \left(\frac{\partial \overline{w}}{\partial z}\right)^2 + \frac{1}{2}\left(\frac{\partial \overline{u}}{\partial y}\right)^2 + \frac{1}{2}\left(\frac{\partial \overline{u}}{\partial z}\right)^2 + \frac{1}{2}\left(\frac{\partial \overline{v}}{\partial z} + \frac{\partial \overline{w}}{\partial y}\right)^2\right]. \quad \text{(A 3)}$$

In $\mathscr{P}_k$, the longitudinal variations of the velocity components have been neglected. The calibration constants in (A 1)–(A 3) are defined according to Rodi (1980) by $c_\mu = 0.09$, $c_{1\varepsilon} = 1.44$, $c_{2\varepsilon} = 1.92$, $\sigma_k = 1.0$ and $\sigma_\varepsilon = 1.3$.

As in the 1DV model, the boundary values for the turbulent kinetic energy at the sidewalls $y = \pm L$ and the bed $z = -h$ are derived from a local equilibrium between production and dissipation of turbulent kinetic energy,

$$\overline{q}|_{z=-h} = \frac{|\boldsymbol{u}_{\star b}|^2}{\sqrt{c_\mu}}, \quad \overline{q}|_{y=\pm L} = \frac{|\boldsymbol{u}_{\star s}|^2}{\sqrt{c_\mu}}. \quad \text{(A 4)}$$

The shear stress velocities $\boldsymbol{u}_{\star b}$ at the bed and $\boldsymbol{u}_{\star s}$ at the sidewalls are determined from the velocity near the wall using a logarithmic law-of-the-wall formulation. The only dependence of the wave motion is via the shear stress velocities. As in the 1DV model, the fluctuating part of the turbulence quantities q and ε is neglected. However, in that model, the eddy viscosity was entirely independent of the wave motion.

Uittenbogaard & Van Kester (1996) developed a boundary condition at the bed and sidewalls for the dissipation rate which is imposed at a distance Δ from the boundary and is independent of the roughness length z_0,

$$\frac{\partial \overline{\varepsilon}}{\partial \psi}(\Delta) = -\frac{|\boldsymbol{u}_\star|^3}{\kappa \Delta^2}, \quad \text{(A 5)}$$

where $\psi = y$ or $\psi = z$ and $\boldsymbol{u}_\star$ denotes the friction velocity at the bed or the sidewall. At the free surface, the turbulent kinetic energy and dissipation vanish. In fact, this concerns the free surface in a Eulerian setting. Since the fluctuating part of the turbulence quantities is neglected, $\overline{q}$ and $\overline{\varepsilon}$ may as well be assumed to vanish at $z = \overline{\zeta}^L$,

$$\overline{q}|_{z=\overline{\zeta}^L} = 0, \quad \overline{\varepsilon}|_{z=\overline{\zeta}^L} = 0. \quad \text{(A 6)}$$

The time integration of the transport equations (A 1)–(A 3) combined with the boundary conditions (A 4)–(A 6) consists of two stages. In the first stage, only horizontal and vertical advective transport is taken into account. The advection terms normal to the boundary are neglected in the computational layer near the bottom and near the sidewalls. In the second stage the remaining non-advective terms are integrated, of which the production, dissipation and diffusion are assumed to be

dominant terms in the transport equation. The vertical transport terms are integrated implicitly.

REFERENCES

Andrews, D. G. & McIntyre, M. E. 1978 An exact theory of nonlinear waves on a Lagrangian-mean flow. *J. Fluid Mech.* **89**, 609–646.

Casulli, V. 1995 Recent developments in semi-implicit numerical models for free-surface hydrodynamics. In *Advances in Hydroscience and Engineering*, vol. 2, pp. 2174–2181. Tsinghua University Press, Beijing, China.

Casulli, V. & Stelling, G. S. 1998 Numerical simulation of 3D quasi-hydrostatic, free-surface flows. *J. Hydraul. Engng. ASCE* **124**, 678–686.

Craik, A. D. D. 1977 The generation of Langmuir circulations by an instability mechanism. *J. Fluid Mech.* **81**, 209–223.

Craik, A. D. D. 1982 The generalized Lagrangian-mean equations and hydrodynamic stability. *J. Fluid Mech.* **125**, 27–35.

Deigaard, R. & Fredsøe, J. 1989 Shear stress distribution in dissipative water waves. *Coastal Engng* **13**, 357–378.

Dingemans, M. W. 1997 *Water Wave Propagation over Uneven Bottoms*. World Scientific.

Dingemans, M. W., Van Kester, J. A. Th. M., Radder, A. C. & Uittenbogaard, R. E. 1996 The effect of the CL-vortex force in 3D wave-current interaction. In *Proc. 25th Intl Conf. on Coastal Engng, Orlando*, pp. 4821–4832.

Grant, W. D. & Madsen, O. S. 1979 Combined wave and current interaction with a rough bottom. *J. Geophys. Res.* **84** (C4), 1797–1808.

Groeneweg, J. & Klopman, G. 1998 Changes of the mean velocity profiles in the combined wave–current motion in a GLM formulation. *J. Fluid Mech.* **370**, 271–296 (referred to herein as GK98).

Kemp, P. H. & Simons, R. R. 1982 The interaction of waves and a turbulent current; waves propagating with the current. *J. Fluid Mech.* **116**, 227–250.

Kemp, P. H. & Simons, R. R. 1983 The interaction of waves and a turbulent current; waves propagating against the current. *J. Fluid Mech.* **130**, 73–89.

Klopman, G. 1994 Vertical structure of the flow due to waves and currents: laser-Doppler flow measurements for waves following or opposing a current. *Tech. Rep. Delft Hydraulics* H840.32, Part 2.

Klopman, G. 1997 Secondary circulation of the flow due to waves and current: laser-Doppler flow measurements for waves following or opposing a current. *Tech. Rep. Delft Hydraulics* Z2249.

Leibovich, S. 1977 On the evolution of the system of wind drift currents and Langmuir circulations in the ocean. Part 1. Theory and averaged current. *J. Fluid Mech.* **79**, 715–743.

Leibovich, S. 1983 The form and dynamics of Langmuir circulations. *Annu. Rev. Fluid Mech.* **15**, 391–427.

Lo, E. Y. & Mei, C. C. 1985 Long-time evolution of surface waves in coastal waters. *MIT Rep. Ralph M. Parsons Lab.* 303.

Longuet-Higgins, M. S. 1953 Mass transport in water waves. *Phil. Trans. R. Soc. Lond.* A **245**, 535–581.

McIntyre, M. E. 1980 Towards a Lagrangian-mean description of stratospheric circulation and chemical transports. *Phil. Trans. R. Soc. Lond.* A **296**, 129–148.

Mei, C. C., Liu, P. L-.F. & Carter, T. G. 1972 Mass transport in water waves. *MIT Rep. Ralph M. Parsons Lab.* 146.

Melville, W. K., Shear, R. & Veron, F. 1998 Laboratory measurements of the generation and evolution of Langmuir circulations. *J. Fluid Mech.* **364**, 31–58.

Nepf, H. M., Cowen, E. A., Kimmel, S. J. & Monismith, S. G. 1995 Longitudinal vortices beneath breaking waves. *J. Geophys. Res.* **100** (C8), 16211–16221.

Nepf, H. M. & Monismith, S. G. 1991 Experimental study of wave-induced longitudinal vortices. *J. Hydraul. Engng ASCE* **117**, 1639–1649.

Nezu, I. & Nakagawa, H. 1993 *Turbulence in Open-channel Flow*. IAHR Monograph, Balkema, Rotterdam.

Nielsen, P. & You, Z-J. 1996 Eulerian mean velocities under non-breaking waves on horizontal bottoms. In *Proc. 25th Intl Conf. on Coastal Engng, Orlando*, pp. 4066–4078.

Peregrine, D. H. 1976 Interaction of water waves and currents. *Adv. Appl. Mech.* **16**, 9–117.

Rodi, W. 1980 *Turbulence Models and their Applications in Hydraulics. A State of the Art Review*. IAHR, Delft.

Uittenbogaard, R. E. & Van Kester, J. A. Th. M. 1996 Modeling seasonal temperature stratification with Triwaq: a preparatory study based on one-dimensional computations. *Tech. Rep. Delft Hydraulics* Z978.

Van Kester, J. A. Th. M., Uittenbogaard, R. E. & Dingemans, M. W. 1996 3D wave–current interaction. *Tech. Rep. Delft Hydraulics* Z751.

Vinokur, M. 1983 On one-dimensional stretching functions for finite-difference calculations. *J. Comput. Physics* **50**, 215–234.

WL|Delft Hydraulics 1999 *User Manual Delft3D-Flow*. Version 3.05.